Design of a Mid-IR Polarimeter for SOFIA

C. Packham[a], M. Escuti[b], G. Boreman[c], I. Quijano[c], J. C. Ginn[c], B. Franklin[c], D. J. Axon[d], J. H. Hough[e], T. J. Jones[f], P. F. Roche[g], M. Tamura[h], C. M. Telesco[a,] N. Levenson[i], J. M. Rodgers[j], J. P. McGuire[j]

[a]Department of Astronomy, University of Florida, 211 Bryant Space Science Center, Gainesville, FL. 32611-2055, USA;
[b]Department of Electrical & Computer Engineering, North Carolina State University, Raleigh, NC 27695-7914, USA;
[c]CREOL, The College of Optics & Photonics, Building 53, University of Central Florida 4000 Central Florida Blvd, Orlando, FL 32816, USA;
[d]Department of Physics, RIT, 84 Lomb Memorial Dr. Rochester, NY, 14623-5603, USA;
[e]Science & Technology Research Institute, University of Hertfordshire, College Lane, Hatfield, AL10 9AB, UK;
[f]University of Minnesota, Department of Astronomy, 116 Church St. S.E., Minneapolis, MN, 55455, USA;
[g]Astrophysics, DWB, Oxford University, Keble Road, Oxford, OX1 3RH, UK;
[h]National Astronomical Observatory of Japan, Osawa, Mitaka, Tokyo 181-8588, Japan;
[i]177 Chemistry-Physics Building, University of Kentucky, Lexington, Kentucky 40506-0055, USA;
[j]Optical Research Associates, Suite 300, 3280 E. Foothill Blvd., Pasadena, CA 91107, USA;

ABSTRACT

Mid-infrared polarimetry remains an underexploited technique; where available it is limited in spectral coverage from the ground, and conspicuously absent from the *Spitzer*, *JWST* and *Herschel* instrument suites. The unique characteristics of SOFIA afford unprecedented spectral coverage and sensitivity in the mid-infrared waveband. We discuss the preliminary optical design for a 5-40μm spectro-polarimeter for use on *SOFIA*, the *SOFIA* Mid-InfraRed Polarimeter (SMIRPh). The design furthers the existing 5-40μm imaging and spectroscopic capabilities of SOFIA, and draws on experience gained through the University of Florida's mid-IR imagers, spectrometer and polarimeter designs of T-ReCS and CanariCam. We pay special attention to the challenges of obtaining polarimetric materials suitable at both these wavelengths and cryogenic temperatures. Finally, we (briefly) present an overview of science highlights that could be performed from a 5-40μm imaging- and spectro-polarimeter on *SOFIA*. Combined with the synergy between the possible future far-IR polarimeter, Hale, this instrument would provide the *SOFIA* community with unique and exciting science capabilities, leaving a unique scientific legacy.

Keywords: Airborne astronomy, Grain alignment, Imaging, Infrared, Instrumentation, Magnetic fields, Polarimetry, Polarization, *SOFIA*, Spectroscopy

1. INTRODUCTION

The Stratospheric Observatory for Infrared Astronomy (*SOFIA*) is the successor to the highly successful, but ~7.5 times smaller Kuiper Airborne Observatory (*KAO*). Offering a near uninterrupted wavelength coverage between 0.3μm to 1.6mm, the 2.5m telescope affords *SOFIA* the status of a premier infrared and sub-millimeter observatory (Becklin 2006). First (airborne) light of the telescope is expected in 2009, with regular science operations expected in 2010. An outstanding suite of nine instruments are approaching, or are already, complete, spanning the wavelength range 0.3μm to 655μm, and offering imaging and low and high-resolution spectroscopic capabilities. Through the very high altitude of

Ground-based and Airborne Instrumentation for Astronomy II, edited by Ian S. McLean, Mark M. Casali,
Proc. of SPIE Vol. 7014, 70142H, (2008) · 0277-786X/08/$18 · doi: 10.1117/12.789843

observations (~12.5km) and its corresponding reduction in precipitatable water vapor, observations in an otherwise opaque part of the atmosphere are possible, opening observations in that wavelength space. Instruments such as FORCAST (Adams et al 2006) fully exploit this capability, in this example offering observing windows throughout the 5-40μm range (Fig. 1, taken from Keller et al 2003).

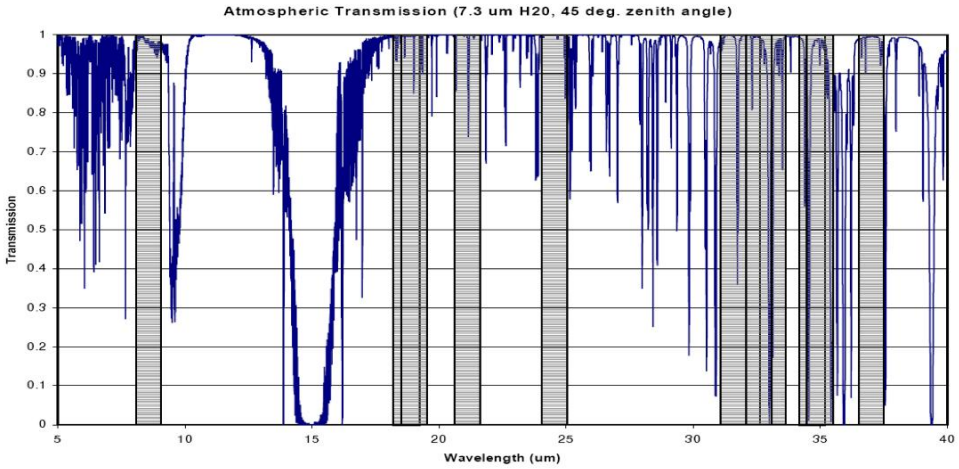

Fig. 1. The atmospheric transmission expected for *SOFIA*, and the shaded areas show the initial filter selection for FORCAST. Figure taken from Keller et al (2003).

Although *SOFIA* provides a huge step forward for IR-submm astronomy, it competes in a rapidly evolving observatory environment. On the ground, observatories such as the twin *Gemini* 8.1m telescopes each have mid-IR (MIR) instruments such as the University of Florida developed T-ReCS (Telesco et al 1998) and Royal Observatory Edinburgh developed Michelle (Glasse et al 1997) providing high spatial resolution observations spanning ~7.5-26μm. In space, the 3.5m *Herschel* telescope, operating at wavelengths of 60-670μm is expected to be launched in 2008, and the 6.5m James Webb Space Telescope (*JWST*), operating at wavelengths of 0.6-27μm has a launch date of 2013. The *SPICA* 3.5m telescope has an expected launch date of ~2017 and will operate at wavelengths of 5-200μm. The very successful *Spitzer* 0.85m and the Japanese *AKARI* 0.7m space telescopes are entering their non-cryogenic observing modes, having made observations at wavelengths between ~3-100μm and ~2-180μm respectively. Finally, the Infrared Space Observatory (*ISO*), with an aperture of 0.6m, operated at wavelengths of 2.5-240μm between 1995-1998. Although *SOFIA* has a relatively modest collecting area in comparison to ground-based telescopes, and still suffers from some strong atmospheric absorption bands compared to space-based observatories, *SOFIA* maintains significant advantages, one of which is through its upgradeability and maintainability. The maintainability, upgradeability and timeliness of *SOFIA* offers new instrumentation the chance to exploit new, novel, or intrinsically more complex instruments that would be excluded from space-based observatories due to the extra risk intrinsic to new techniques, technologies and complexities. Through exploiting the wavelength regime unobtainable from the ground and using state of the art and novel instrumentation, *SOFIA* will open new vistas in astronomy.

Polarimetry, whilst proving fundamental to the understanding of astronomical objects as diverse as galaxies and AGN, star formation regions, and debris disks, has rarely been deployed on space-based telescopes, with notable exceptions including *ISO* and the Hubble Space Telescope (*HST*). The dominant reason for the exclusion of polarimeters has not been due to a lack of science drivers, rather it has been due to the extra and regular motion of additional mechanisms or telescope pointing, providing extra areas of risk, enhanced demand on cryogens and more complex instruments. Such considerations are always paramount in the consideration of space-based instruments, and this serves to favor a more conservative approach to instrumentation. Such a concern is very significantly moderated on *SOFIA*, as it will return to the ground at the end of each observing night, mitigating fears that malfunctioning mechanisms can lead to lost science potential, as any such problems can be repaired during the day, or the instrument can be replaced with another until repairs can be made. In this paper, we discuss several science cases for a second generation *SOFIA* instrument, a MIR imaging- and spectro-polarimeter, an instrument that would fill a unique niche in astronomy for the *SOFIA* community. The rest of this paper is set out as follows. In section 2 we provide an overview of the polarimetric processes that are important at MIR wavelengths, along with brief specific examples (a more detailed description of example science cases can be found in Packham et al 2007). In section 3 we discuss a new breed of optics components that will offer the key

polarimetric functionality, and we detail their testing and characterization at 5-40μm. In section 4 we discuss a conceptual design offering spectropolarimetry and total flux imaging only, but which we believe in a latter stage can be extended to offer imaging polarimetry. Finally we draw conclusions and discuss future work in section 5.

2. ASTROPHYSICAL POLARIMETRY

Polarization in the MIR is usually due to emission and absorption by aligned aspheric dust grains; polarization due to scattering from typical (astrophysical) sized dust is not observed at wavelengths >5μm. The polarization gives access to the presence, orientation and distribution of magnetic fields in astrophysical objects, and the nature and mineralogy of the dust grains in them and in the interstellar medium, and is much more sensitive to chemical and physical differences than spectroscopy alone. Such polarimetry has so far only been done using ground based telescopes and consequently has been limited in spectral coverage and sensitivity and is very weather dependent. Despite these challenges, early work detected and measured the orientation of magnetic fields in a number of star forming regions, YSO's, the inner central region of the Galaxy, SgrA, a Seyfert galaxy and sundry other objects, with a range of dust chemistries involved, in all totaling some 30 or so objects.

Polarimetry can be used to determine magnetic field geometries as dust grains appear to align in many, or perhaps most, astrophysical situations. Although the alignment process is often unclear there is general agreement that, because of the Barnet effect, the short axis of the grains will be aligned with the local magnetic field. The position angle (PA) of polarization provides the direction of the magnetic field, where the magnetic field is parallel to the polarization vector for absorptive polarization, and perpendicular for emission polarization. Where the grains have a preferential alignment, the polarization is attributed to differential extinction (or emission in the case of longer wavelength observations) between two orthogonal directions along the line of sight, leading to dichroic extinction (or emission at longer wavelengths). In the case of stellar formation, the PA of polarization is often compared with symmetry axes, such as the disc and/or the outflow axes, in order to investigate the precise role of the magnetic field in the formation process.

As noted above, the PA of polarization is perpendicular in the two forms of dichroism, offering a clear diagnostic if the wavelength range is large enough. Indeed, in many cases MIR polarimetry can detect two polarization components in the same object, at different locations from the exciting source. The first is from dichroic absorption from cold dust (≤150K) and the second from emission by warm (≥150-550K) dust, where the flux is emitted at different locations from the exciting source. Observations at other wavelengths often detect only one form of polarization, or can be complicated through the superposition of two, or sometimes three polarizing components. For MIR polarimetric observations, models exist (Aitken et al 2002) to determine magnetic field geometries in disks from the observed polarization.

Despite the limited number of observations, grain alignment seems to be ubiquitous. Objects as diverse as the outer regions of diffuse clouds, dense and massive molecular clouds, the interstellar medium, HII regions and galaxies/AGN all exhibit strong grain alignment. As many have noted, major progress in this area is limited by access to the necessary instrumentation, both in the availability of polarimetric observations and the breadth of the wavelength range offered by those instruments. With the breadth of wavelength coverage for the proposed *SOFIA* based polarimeter, the 90° PA of polarization switch which occurs between dichroic absorption and emission can be easily identified, enabling the optical thickness of disks around young stars and AGN to be determined (Efstathiou et al 1997).

The emission of the inner regions of the circumstellar envelope in the post AGB phase peaks in the MIR, with dust temperatures ~150-200K. MIR polarimetry can therefore provide a powerful means to detect and study any magnetic field in these regions. Significant work has been achieved on such objects (e.g. Gledhill, 2005), but these are confined to 2 and 850μm. Whilst ground based polarimeters on 8m class telescopes will extend the wavelength range to ~14μm, and the proposed *SOFIA* based Hale (Dowell et al 2003) will operate at wavelengths ~50μm and longer, there will still be a very significant gap in coverage of the wavelength space, critical as the wavelengths between 5-40μm will spans the change from dichroic absorption to emission for many objects.

Spectropolarimetry is a particularly powerful diagnostic as it can separate the emissive and absorptive components, which is not usually possible from the total flux spectrum, and the properties of the dust grains can be determined by detailed fits to the polarization spectrum. Furthermore, the polarization spectrum, unlike the intensity spectrum, is independent of the nature of the underlying source, so long as this is unpolarized. Even if this latter condition is not satisfied, polarization in the underlying source, or variations in chemistry along the line of sight, is usually revealed by changes in PA through the spectrum. Since the intensity and polarization spectra are different functions of the optical

constants of the grain material, spectropolarimetry gives additional and independent information about the physical and chemical structure of grains and their mantles.

To date, only the silicate feature in the 10μm window has been studied in any detail. Spectropolarimetry of the 20μm feature has only been carried out for a few bright objects (see Smith et al 2000) and no consistent modeling of both features has been made. The extra sensitivity in the 20μm band with a SOFIA based polarimeter will allow modeling of the silicate feature for far more objects and hence show whether BN is peculiar or there is a fundamental problem in understanding the nature of the grains responsible for the ubiquitous 10 and 20 μm features.

The extended wavelength coverage will allow spectropolarimetry of several other features. Although the 3μm ice feature (OH stretch), the most common constituent of interstellar grain mantles, can be observed from the ground, the features at 6μm (OH bend) and 13.5 μm (libration mode) cannot. The features, identified primarily with water-ice, also contain many other molecules although their identification is not always clear.

The growth of dust grains in protoplanetary disks, a process that must occur as planetesimals, and eventually planets, form, is an area of much current interest. There is evidence for grain growth in the disks around T Tauri and Herbig Ae/Be stars, with the flatter 10μm silicate feature suggesting the presence of particles larger than 2μm (van Boekel et al 2005). However, flat 10μm spectra can also be produced for porous grains of size ≤0.3μm (Voshchinnikov et al 2006). Porous grains are likely, particularly in debris disks, where the dust probably originates from comets and might well be similar to the interplanetary dust particles collected from the upper atmosphere of the Earth. Polarimetry can distinguish between the two models as large particles will have significant albedo (0.3-0.4) and will produce large polarization (several %) from scattering. Spectropolarimetry of different age disks will be particularly useful in studying the nature of dust grains and the growth in grain sizes.

3. POLARIZATION GRATINGS

An optimal design for a polarimeter must minimize temporal atmospheric effects, typically accomplished through modulating the polarimetric signature faster than typical sky variations (both sky transmission and emission), and minimize instrumental polarization. At wavelengths from optical to MIR, astronomers have used dual-beam polarimeters, such as those deployed on the *AAT* (Hough et al 1994), *UKIRT* (Davis et al 2005) and *MMT* (Packham & Jones 2008). Typically, a crystalline Wollaston prism and half wave retarder have been used, offering very high throughput, low instrumental polarization and high accuracy. However, CanariCam (Packham & Telesco 2007), the soon to be commissioned instrument that includes a dual-beam polarimeter for the 10.4m *GTC* telescope, may be the longest wavelength polarimeter that makes use of a crystalline Wollaston prism. At wavelengths longer than ~20μm, there appears to be no suitable birefringent crystalline materials for a Wollaston prism and half wave retarder.

A novel polarizing beamsplitter using birefringent gratings (Oh & Escuti, 2007, Escuti et al 2006) is being pioneered at North Carolina State University (NCSU). The key optical element is called a polarization grating (Tervo & Turunen 2000), which is a thin-film beamsplitter that is functionally analogous a Wollaston prism (see Fig. 2a-c), although it operates on a completely different principle. The beamsplitter is made up of a thin polymer film (<300μm) comprising a liquid crystal polymer coated optionally on a reflective or transparent substrate, and can be made with almost any surface area. The essential structure of these polarization grating (PGs) is implemented using uniaxially birefringent, polymerizable, liquid crystal materials (Kelly 1995), arranged into a continuous, in-plane, bend-splay pattern (an example of which is shown in Fig. 2d). This pattern is established using a UV polarization hologram exposing photo-alignment materials (Escuti et al 2006, Schadt et al 1996), followed by spin-coating of the polymerizable liquid crystal. Although its natural eigen-polarizations are circular (i.e. *V*), the PG beamsplitter can be paired with a quarter waveplate (QWP) in order to separate incident light based on any eigen-polarization desired (e.g. *Q*, *U*) (Escuti et al 2006), as illustrated in Fig. 2e.

At optical and near-infrared wavelengths, PG diffraction efficiency has been shown to be >99% (nearly no absorption or scattering), diffracting incident light into one of only three orders (m=0, ±1) based on the incident polarization state (see Fig. 2a-c). In NCSU's nearly ideal experimental gratings, the m=0 beam is unpolarized, but contain typically <0.5% of the incident flux when optimized for visible wavelengths (Escuti & Jones 2006), and <0.125% when optimized at 1550nm (Kim et al 2008). The m=±1 orders are very highly perpendicularly polarized (>99%), making the PG component a potentially ideal alternative to other analyzers. Note that while Fig. 2 shows the transmissive configuration, the reflective mode is completely analogous (Komanduri et al 2008). As the component is a grating, the

resulting beams are sorted into polarization state as well as spectrally dispersed, as shown in Fig. 2e, following the classic grating equation ($\sin\theta_m = \lambda/\Lambda$, where Λ is the grating period and θ_m is the diffraction angle of order m). Polarization gratings are currently being developed at NCSU as polymer films and electrically-switchable diffractive elements for ultra-efficient liquid crystal displays, non-mechanical optical beam-steering, and telecommunication devices, variously funded by the National Science Foundation and the US Air Force Research Laboratory, among others.

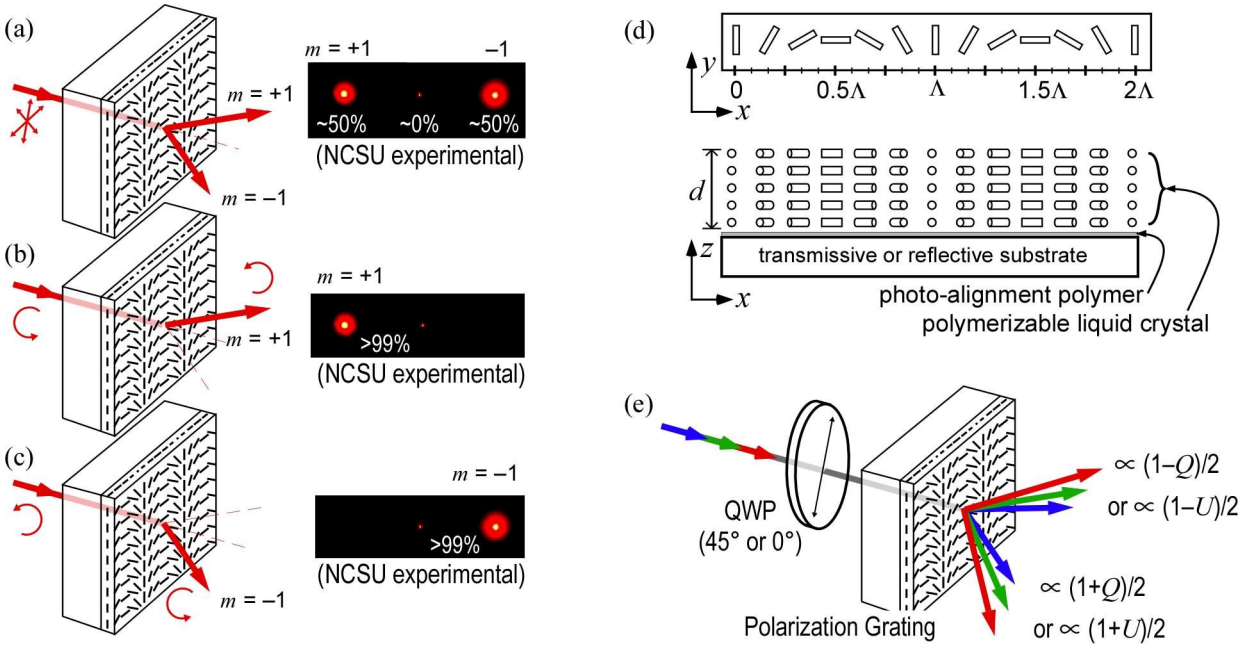

Fig. 2. Polarization grating (PG) behavior: (a) incident linear or unpolarized light splits equally into the two first orders; incident (b) left- and (c) right-circularly polarized light diffracts fully into only one of the first orders; (d) top- and side-views of the nematic director structure; and (e) arrangement with a quarterwave-plate (QWP) sensitizing diffraction to linearly polarized light (i.e. Q and U).

Here we report our preliminary work as we consider the behavior of PGs at MIR wavelengths (5-40μm). We assert that two primary questions drive this initial work: (i) Do our current polymerizable liquid crystal materials manifest any birefringence over this wavelength range? and (ii) What is the absorption over this wavelength range? With answers to these questions, we can estimate the overall throughput of PGs at 5-40μm.

The indices of refraction and the extinction coefficients of the uniaxial birefringent liquid crystal polymer (RMS03-001C, from EMD Chemicals, ~10μm film thickness) were measured on a J. A. Woollam Infrared Ellipsometer System at CREOL. All measurements were performed at room temperature. From the measured ordinary n_o and extraordinary n_e indices, the birefringence $\Delta n = n_e - n_o$ was found, which is shown in Fig. 3a along with the measured extinction coefficient k. Notice that a strong birefringence (~0.15) is indeed present, a value that compares very favorably to that offered by crystalline materials at optical and near-IR wavelengths (e.g. Perrin et al 2008). Note also that the extinction coefficient is particularly low at wavelengths >~20μm, the very range at which conventional crystalline Wollaston prisms no longer function. The absorption coefficient ($\alpha = 4\pi k/\lambda$) is shown in Fig. 3b.

The total throughput T_{tot} of the PG thin-film is composed of several elements, and may be estimated in both reflective and transmissive modes by the following:

$$T_{tot} = \eta_{eff}\eta_{abs}\eta_{refl} = \eta_{eff}\exp(-\alpha d)(1-R)^2, \qquad (1)$$

where η_{eff} is the diffraction efficiency of the grating itself, to be calculated below. The quantity $\eta_{abs} = \exp(-\alpha d)$ is the fraction of light not absorbed through a film of thickness d (which must be $d \sim 3\lambda_0/(2\Delta n)$, as discussed below). The quantity $\eta_{refl} = (1-R)^2$ is the fraction of light not reflected at the two air-polymer interfaces, where the reflectance of each interface determined by the Fresnel equation $R = ((n-1)^2 + k^2)/((n+1)^2 + k^2)$, shown in Fig. 3b for our measured n and k.

For simplicity, we have neglected the influence of the substrate, which in reflective PGs is likely to be only a refinement on the estimate in Eq. (1).

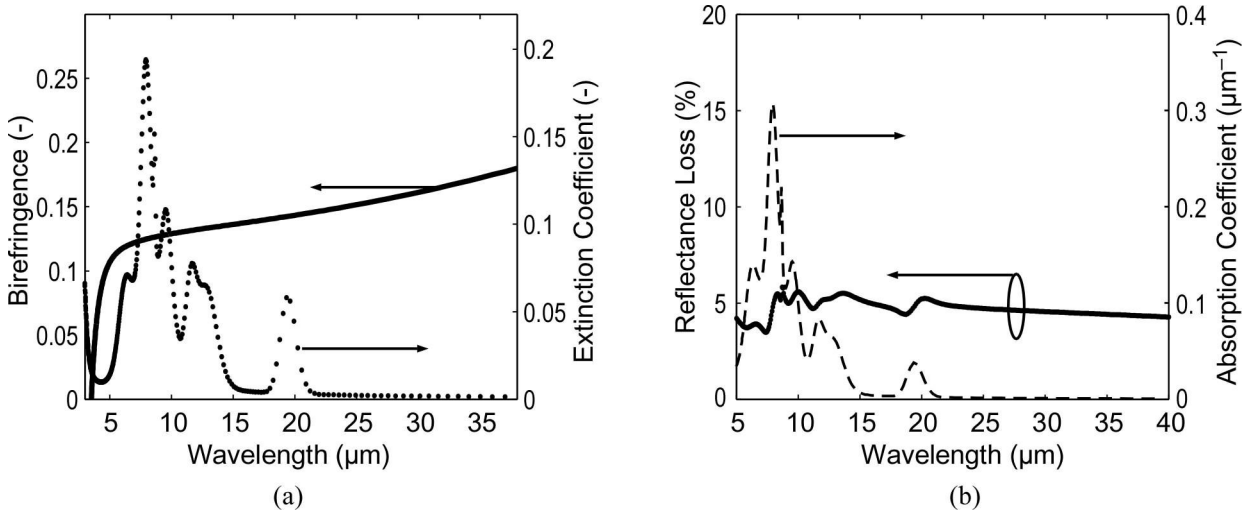

Fig. 3. Preliminary measurements on RMS03-001C liquid crystal polymer films: (a) birefringence and extinction coefficient; and (b) Fresnel interface reflectance loss and absorption coefficient.

The diffraction efficiency of the conventional PG profile illustrated in Fig. 2d is well known to be >99% in both theory and experiment (Oh & Escuti 2007, Escuti et al 2006), but only at wavelengths close (within $\Delta\lambda / \lambda_0 \sim 12\%$) to the halfwave retardation condition ($\lambda_0 \sim 2\Delta nd$). Nevertheless, several 'achromatic' PGs with modified nematic director profiles have been identified (Oh & Escuti 2008), with high efficiency bandwidths $\Delta\lambda / \lambda_0$ increased by up to eight-fold. In the most preferred achromatic PG for this application, the thickness depends on the center wavelength of the high efficiency window according to $d \sim 3\lambda_0/(2\Delta n)$. In Fig. 4a, we show the calculated diffraction efficiency of three achromatic PGs using the Finite-Difference Time-Domain (FDTD) simulation tool *WOLFSIM* (Oh & Escuti 2006). These three wavelength windows (5-11.2μm, 11.2-25μm, and 25-40μm) were chosen based on the FPA detector technologies (discussed in the section 4) and the desire to keep the spectral dispersion consistent. The ideal PG diffraction efficiency η_{eff} is therefore >99% for the entire 5-40μm range.

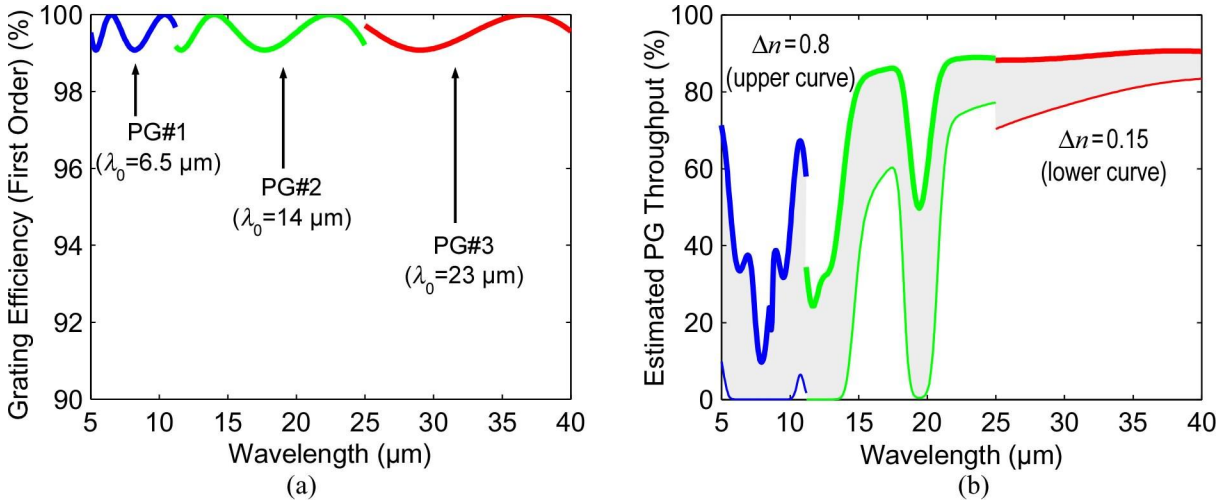

Fig. 4. (a) First-order grating efficiency calculated using FDTD numerical simulation; and (b) Estimated total throughput of a polarization grating formed with the initial liquid crystal polymer RMS3-001C (lower curve), and when doped with nano-particles (upper curve).

In Fig. 4b, we estimate the total PG throughout T_{tot} via Eq. (1), the data in Fig. 3, and the calculation in Fig. 4a. The lower curve represents the data where $\Delta n \sim 0.15$, which is the birefringence from our initial measurements on the current

liquid crystal materials (which were developed for visible wavelengths). In this case, the three PGs have thicknesses of 65, 140, and 230μm in order to meet the high diffraction efficiency condition. While good throughput occurs at wavelengths >15μm, a much lower throughput occurs at lower wavelengths (entirely due to absorption). It is important to note that many optimization techniques are known in the liquid crystal community that can enhance materials to increase the birefringence while decreasing absorption, including modified chemical structures and guest-host doping with nanoparticles. One of the avenues we are studying involves doping with single-walled carbon nanotubes (Fagan et al 2007), which manifest very low absorption and very high birefringence at 5-40μm. Our best estimate is that this approach could lead to birefringence values around $\Delta n \sim 0.8$, enabling much thinner PGs (thicknesses of 12, 26, and 43μm). Under this assumption, we show the revised total throughput in Fig. 4b as the upper curve, a marked improvement, with high-to-modest throughput.

It is important to note that both the initial fabrication of and measurements on the liquid crystal polymer measured above were all made at room temperature. Nevertheless, the optical and mechanical behaviors of PGs at the operational cryogenic temperatures are undoubtedly critical for SMIRPh. Whilst we are still in the initial phase of studying temperature effects, we can note two points: (1) The liquid crystal material composing the PG is a highly cross-linked poly-acrylate network, which we have observed to remain mechanically intact even with manual handling at liquid nitrogen temperatures; and (2) It is well known that the birefringence of these materials increases as temperature decreases (Broer et al 1989). With both of these positive points in mind, we are actively working to quantitatively understand the optical/physical behavior and limitations of our polymer PGs at cryogenic temperatures.

In summary, we have shown that PGs show the necessary birefringence at the MIR wavelengths of operation. Future work will continue optimization work on the transmission of the PGs, and refining our preliminary measurements, which are likely pessimistic as the absorption bands are likely significantly more narrow than we show above. At the time of writing, we are currently working on an optimized MIR PG and will report the transmission and birefringence results in a later publication. Finally, we plan to characterize the PGs at cryogenic temperatures. At the conceptual level of this design study, we have shown that SMIRPh can indeed by based around PG technology and in the next section we produce an optical design based on PGs.

4. CONCEPTUAL DESIGN

In the following section, we discuss the conceptual design for a *SOFIA* based instrument using the polarization gratings as both the analyzer and modulator. They key goal of the design was to investigate the applicability of polarization grating technology to a *SOFIA* instrument, and so several assumptions were made that need to be refined in any follow-on preliminary or critical design phase. Further, as the detector number of pixels and their size play a fundament role in the design, we have base-lined the optical design using reasonable assumptions based on current array development. The key design inputs are:

1. Two spectral bands are required, spanning 5-25μm and 25-40μm, henceforth the blue and red arms respectively
    a. The 5-25μm array is based-lined around Raytheon's Aquarius array, a 1024^2 Si:As based detector
    b. The 25-40μm array is base-lined to be the same pixel size and number as the Aquarius, likely a Si:Sb array
2. If possible, simultaneous observations in the red and blue arm with a minimal transition in wavelength space between the arms
3. The optics must be diffraction limited at all wavelengths >15μm, the shortest wavelength at which *SOFIA* is expected to deliver diffraction-limited observations
4. The plate scale is set to Nyquist sample the shortest wavelength at which *SOFIA* is expected to deliver diffraction-limited observations
    a. In the blue arm, this is at λ=15μm, resulting in a plate scale of 0.62" per pixel
    b. In the red arm, this is at λ=25μm, resulting in a plate scale of 1.03" per pixel
5. Instrument must be a dual-beam polarimeter to maximize efficiency and minimize spurious polarization due to variable sky transmission, emission and image quality
    a. Images in orthogonally polarized beams must be of indistinguishable image quality to ensure minimal instrumental polarization
6. Instrumental polarization must be low (<1%)
7. Imaging- and spectro-polarimetry should be available, with [total flux] imaging available as a goal
8. Spectroscopic resolution optimized to disperse entire wavelength window on each array

9. The system should be an all reflective design, as far as possible, to minimize chromatic aberrations
10. Optics must be readily able to be fabricated
11. The instrument must conform to the *SOFIA* space envelope

The design of the instrument initially aimed to disperse the spectra in wavelength space across one array (e.g. horizontally) and the orthogonally polarized beam offset (e.g. vertically dispersed on the array). However, the particular polarization grating tilt, the space envelope and drive to have the images in the orthogonally polarized beams indistinguishable from each other would have lead to optics that were extremely difficult, if not impossible, to manufacture. At the conceptual design phase, we choose to implement two arms per polarimetric plane in addition to the two color channels. Whilst this inevitably requires more optics and four arrays, economies of scale will significantly reduce the optics costs, and streamlining of the array and readout electronics may also realize cost savings. We further note that the conceptual design aimed to initially prove that polarization gratings offered a viable optical solution at the wavelengths of operation, and that an instrument that meets the above requirements is feasible. In a later design phase, the trade-offs between a single detector per wavelength space vs. cost will be fully investigated.

The coatings on the *SOFIA* dichroic beamsplitter will likely dominate the polarization properties of that optical component, but we have been unable to obtain sufficient information on this device to well characterize it, and hence we plan to confirm the effects on the final instrumental polarization in a later design phase. At this stage, we model the 45° protected gold dichroic mirror, and estimate the polarization vs. wavelength based on *SOFIA's* technical specifications of the coating (Fig. 5). We estimate that this components acts as a 2-6% polarizer, and retards the beam between 3-8%, both effects are strongly wavelength dependant. To reduce the instrumental polarization, a static compensating mirror is used to minimize this effect.

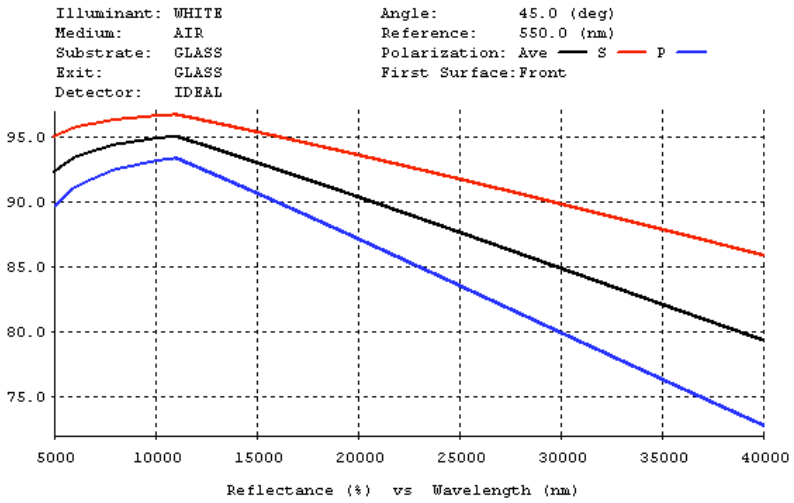

Fig. 5. Estimate of the transmittance vs. wavelength of the dichroic in the orthogonally polarized beams, and the average.

The overall optical system consists of the *SOFIA* telescope and the optical instrument package. The *SOFIA* telescope forms a F/19 image at a slit or a field stop. The optical instrument package consists of elements that relay the slit or field stop onto a detector, in image mode or imaging spectro-polarimeter (ISP) mode.

The instrument optics include the following key elements or groups:

1) A conic mirror collimator that forms a 95 mm diameter collimated beam and an accessible intermediate pupil (image of the *SOFIA* primary mirror).

2) A dichroic beamsplitter that reflects the 5-25μm spectral band, and transmits 25-40μm band.

3) A rotating quarterwave plate in each spectral channel (two total) that functions as a half wave retarder plate upon reflection. It is rotated in steps to several angles between 0° and 90°.

4) A polarization grating (PG) in ISP mode, or flat mirror in imaging mode, at the pupil formed by the collimator in each spectral channel. In the ISP mode, the PG diffracts the S polarization state into the +1 order, and the P polarization state into the -1 order. The grating is oriented so that +1 and -1 orders are diffracted symmetrically

about the grating surface normal. Thus the field angles emerging from the grating are the same in the +1 and -1 orders. See Fig. 6 for an illustration of the symmetric diffraction. In imaging mode, each grating is replaced by a flat mirror tilted so that the light reflects in the same direction as one of the diffracted orders.

5) A set of four 3-conic-mirror objectives (one objective each for long wave and short wave sides, and for +1 and -1 diffracted orders from the PG). Each objective collects the collimated field of view emerging from the grating or flat mirror and forms an image across the detector. In the imaging mode, in which the grating is replaced by a flat mirror, only two of the objectives are used in forming an image. Because the short wave and long wave channels have different plate scales and fields of view, the imager designs for these bands are different. However, in each spectral band, the imager designs for +1 and -1 diffraction order are identical.

Fig. 7 and Fig. 8 show layouts of the instrument optics from different perspectives, with key elements labeled. All mirrors are conics and can be fabricated by diamond turning on aluminum substrates. Mirrors of this type are routinely fabricated by several different experienced vendors. Although the overall system consists of 13 powered mirrors, alignment is not expected to be unusually difficult because of the modular nature of the configuration and the computer-controlled fabrication method planned for the mirrors and mounting structure. Alignment features can be machined into the parts to enable accurate initial alignment. The details of the alignment will be worked out by the engineering team at a later date, but conceptually, the system can be built up step by step beginning at the telescope prime focus. The collimator will first be aligned to the slit using an interferometric test. Each 3-mirror objective will be separately aligned as an independent unit. At these long wavelengths, the mirror placement tolerances in the objective are expected to be in the 50-100μm range which is considered moderate. Final alignment of each 3-mirror assembly can be done by adjusting one mirror in an interferometric test, which is a standard method commonly used by several vendors. Each fully aligned 3-mirror objective will then be added to the instrument package and oriented to accept the collimated beam emerging from the collimator and grating or flat mirror. Because the interface between collimator and imager is in collimated space, the placement tolerance of each imager will be inherently loose, probably on the order of hundreds of microns in position, and a few arc minutes in angle.

Fig. 9 shows how the slit in ISP mode is dispersed across the focal plane, for one of the four focal planes (here, one of the long wave FPAs is shown). The active area of the FPA, 1024x1024x30μm pixels, is filled in both the dispersion and slit directions. We require a total of two polarization gratings to span the wavelength range of interest, as discussed above. In the blue arm, we subdivide that arm into two wavelengths. This is necessary as we wish to use all detector pixels and minimize system complications, and we require the same dispersion and the same average dispersion angle. The spectral dispersions are shown in Table 1 below.

Operational Wavelength	Wavelength of Calculated Dispersion	Dispersion
25-40μm	32.574μm	14.87nm pixel^{-1}
5-11.2μm	8.120μm	6.91nm pixel^{-1}
11.2-25μm	18.102μm	14.35nm pixel^{-1}

Table 1. Spectral dispersion at the noted wavelength in the three spectral arms.

The design-only wavefront performance is diffraction limited at the wavelengths of interest (15μm in the short wave band and 25μm in the long wave band). Fig. 10 shows plots of the parameter 1-SR (where SR is the Strehl ratio) across the square field of view in the imaging modes of the short and long wave bands. In Fig. 10, the diameter of the circles indicate the value of 1-SR at an array of field points, and a smaller diameter indicates better performance. In the long wave band at 25μm wavelength, the Strehl ratio is 0.85 or more. In the short wave band at 15μm wavelength, the Strehl ratio is 0.93 or more. The conventional definition of diffraction limited is 0.80 Strehl ratio.

The polarization analysis is in progress pending receipt of coating data for the dichroic beamsplitter. The 45° tilted tertiary mirror in the *SOFIA* telescope currently is estimated to introduce up to 8° of retardance which is significant relative to the goal on the instrument polarization. To compensate the effects of this mirror, the design team plans to place a flat mirror after the prime focus tilted in a direction that is out of plane to the tilt of the tertiary, as shown in Fig.11. In Fig. 12 we show the SMIRPh layout and space envelope, showing the optical design easily fits within that envelope. Future work will confirm that the supporting mechanical and electrical components will not overfill the envelope.

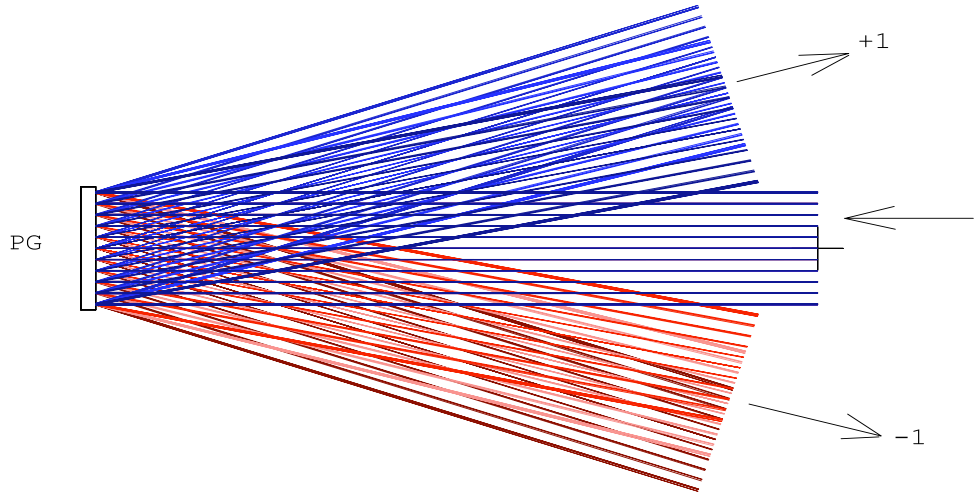

Fig. 6. Polarization grating diffracts S state into +1 order and P state into -1 order, symmetrically about the grating surface normal.

.

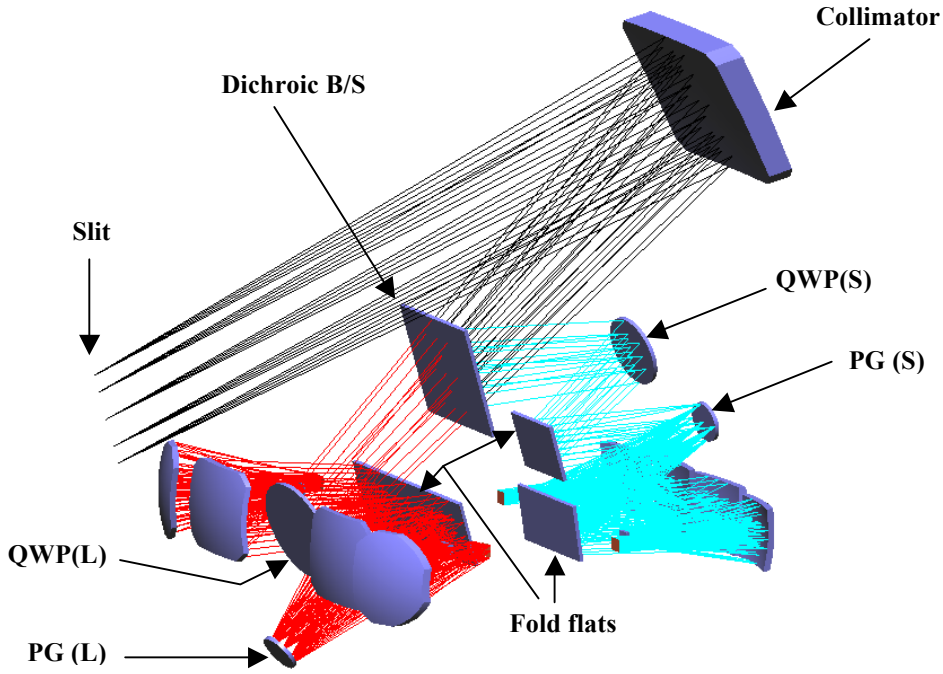

Fig. 7. Layout of optical instrument in Imaging Spectro-polarimeter mode

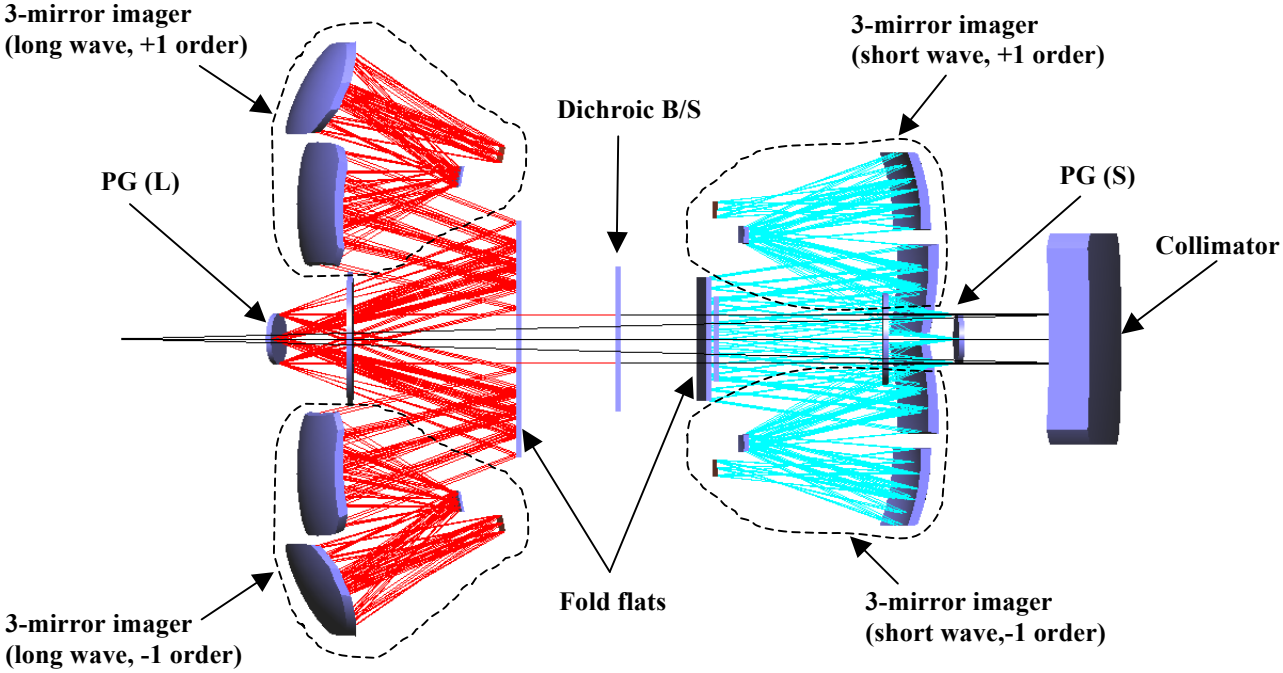

Fig. 8. Layout (top view) of Imaging Spectro-polarimeter mode

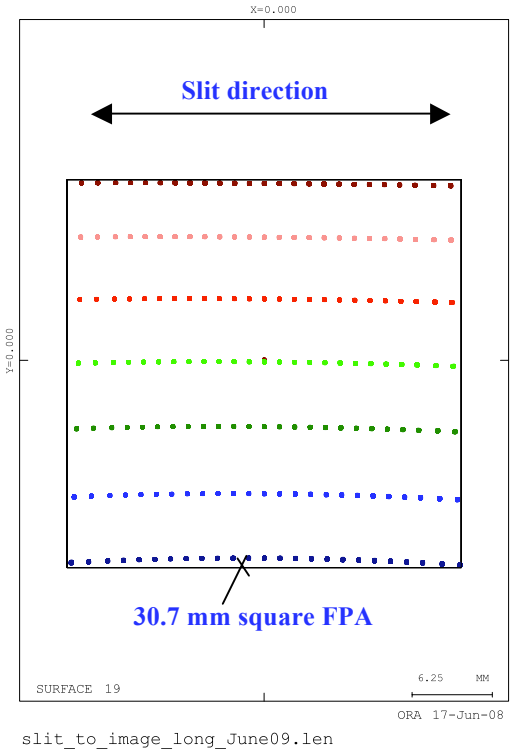

Fig. 9. Dispersion of slit across the detector array; 7 LW wavelengths shown

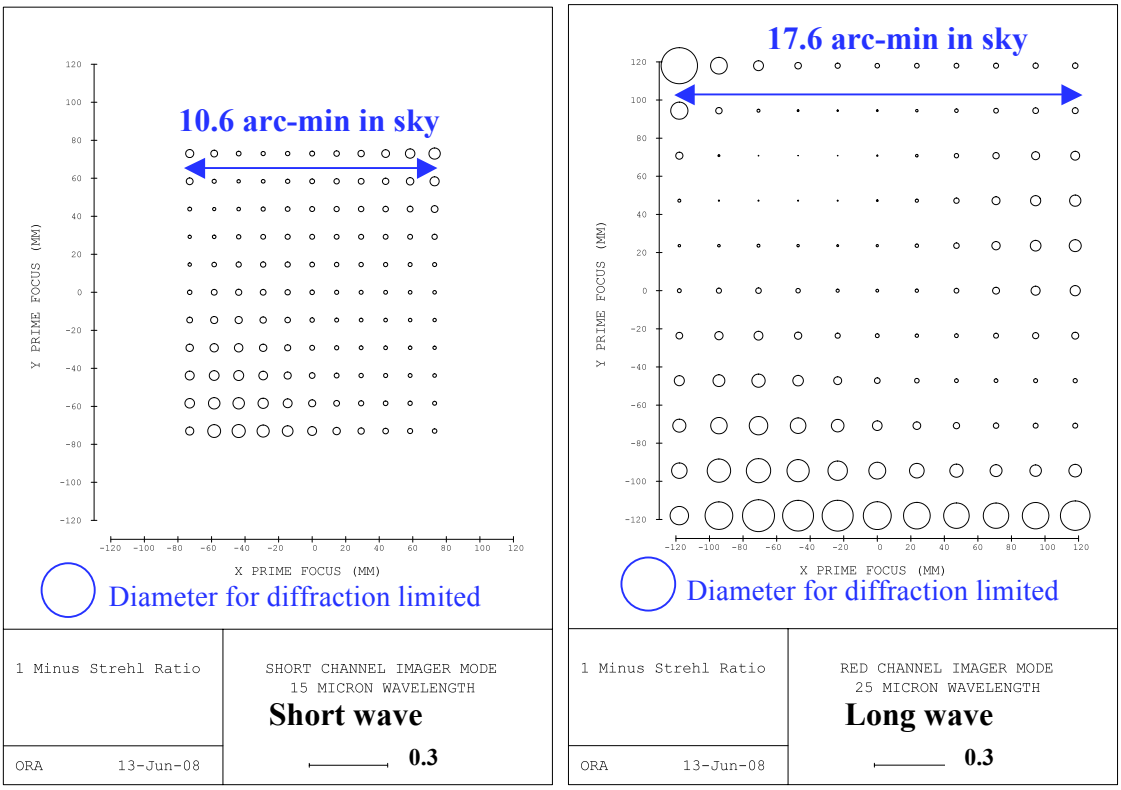

Fig. 10. Field map of "1 minus Strehl ratio" at field angles across the square field of view in imaging mode, short wave (left) and long wave (right). Larger diameter of the circle indicates worse image quality.

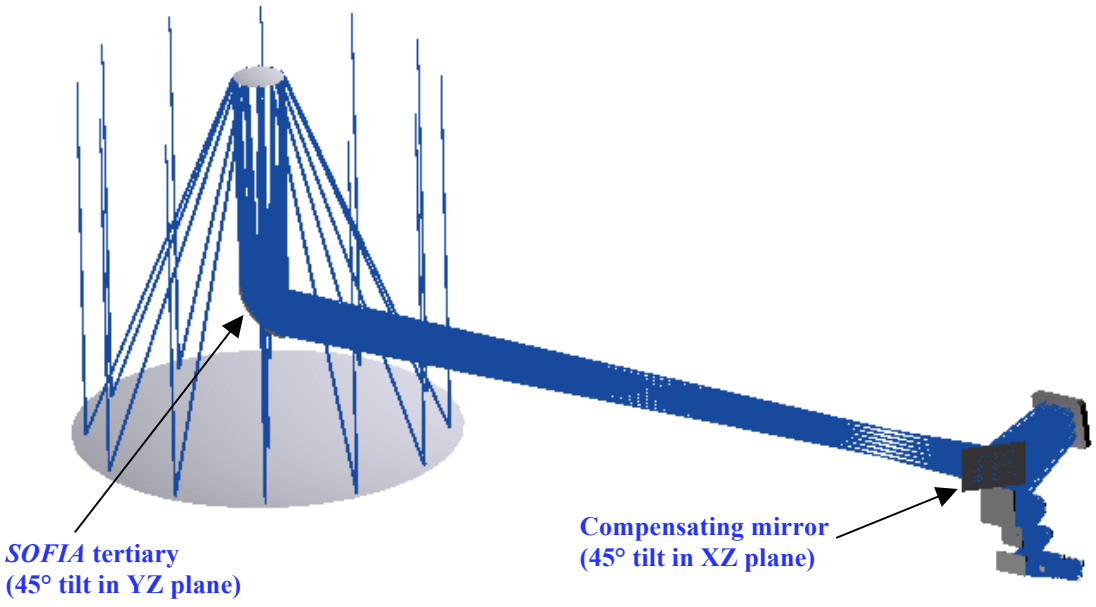

Fig. 11. Layout showing the planned method for compensating the polarization effects of *SOFIA* tertiary.

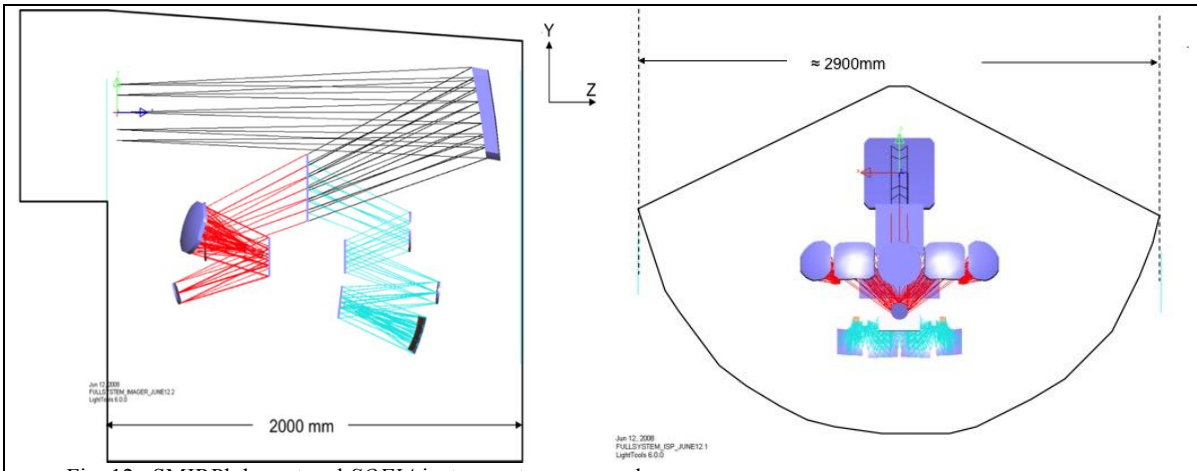

Fig. 12. SMIRPh layout and *SOFIA* instrument space envelope.

5. CONCLUSIONS & FUTURE WORK

In this manuscript we have briefly described the broad and important science cases that polarimetry across 5-40µm can deliver. The combination of SMIRPh and the possible 50-200µm polarimeter on *SOFIA* (Hale, Dowell et al 2003), would provide a unique scientific legacy for the astronomical community, unparalleled on any current or projected ground- or space-based observatory. We also show that the new and novel polarization grating technology can be readily extended to the 5-40µm wavelength region, offering the most promising device to perform both the polarimetric modulation and analysis. Whilst the choice to implement two arms per polarimetric plane in addition to the two color channels will increase costs, the conceptual design aimed to prove that polarization gratings offered a viable optical solution at the wavelengths of operation, and that an instrument that meets the above requirements is feasible. In a later design phase, the trade-offs between a single detector per wavelength space vs. cost will be fully investigated. We note that this optical design successfully implements polarization grating technology for the first time into an astronomical instrument, ensuring diffraction limited observations at all wavelengths that *SOFIA* will deliver such images. Our design offers both total flux imaging and imaging spectropolarimetry; in a future design phase we plan to investigate the feasibility of implementing imaging polarimetry using PGs within the *SOFIA* space envelope.

To continue this work, we urge the *SOFIA* project office to move as expeditiously as possible to opening the proposal phase for the second generation instruments, where our initial focus of work will be on the mechanical and electrical/array designs. It is our belief that *SOFIA* can offer a unique niche due to the unusual capabilities inherent in an airborne observatory. We note that that SMIRPh meets many of the criteria that the *SOFIA* observatory plans to offer, including (a) providing ground-breaking science, (b) opening new windows and observing techniques, (c) providing a technology proving station for new and novel instrumentation, in preparation for future space-based deployment, and (d) providing the opportunity for instrument builders/developers and their graduate students access to state-of-the-art astronomical facilities. Finally, we note that the instrument and the technologies used are of significant interest to the remote sensing and military communities.

6. ACKNOWLEDGEMENTS

CP acknowledges the helpful discussions with Rachel Mason, Stuart Young, Kevin Thompson and Noboru Ebizuka that have improved this paper. We wish to thank the generous support of the UCF-UF Space Research Initiative for enabling this research to take place.

REFERENCES

[1] Becklin, E. E., 2006, 36th COSPAR Scientific Assembly, 36, 672
[2] Adams, J. D., et al 2006, SPIE, 6269, 34
[3] Keller, L. D., Herter, T. L., Stacey, G. J., Gull, G. E., Schoenwald, J., Pirger, B., & Nikola, T. 2003, SPIE, 4857, 29

[4] Telesco, C. M., Pina, R. K., Hanna, K. T., Julian, J. A., Hon, D. B., & Kisko, T. M. 1998, SPIE, 3354, 534
[5] Glasse, A. C. H, Atad-Ettedgui, E. I., & Harris, J. W., 1997, SPIE 2871, 1197
[6] Packham, C. C., Axon, D. J., Hough, J. H., Jones, T. J., Roche, P. F., Tamura, M., & Telesco, C. M., 2007, SPIE, 6678, 66780F
[7] Aitken, D. K., Efstathiou, A., McCall, A., Hough, J. H. 2002, MNRAS, 329, 647
[8] Efstathiou, A., McCall, A., Hough, J. H. 1997, MNRAS, 285, 102
[9] Gledhill, T. M. 2005, Astronomical Polarimetry: Current Status and Future Directions, 343, 243
[10] Dowell, C. D., Davidson, J. A., Dotson, J. L., Hildebrand, R. H., Novak, G., Rennick, T. S., & Vaillancourt, J. E., 2003, SPIE, 4843, 250
[11] Smith, C H, Wright, C M, Aitken, D K, Roche P F, Hough, J H, 2000. MNRAS 312, 327
[12] van Boekel R et al, 2005, A&A, 437, 189
[13] Voshchinnikov NV et al, 2006, A&A 445, 167
[14] Hough, J. H., Chrysostomou, A., & Bailey, J. A., 1994, ASSL, 190, 287
[15] Davis, C.J., Chrysostomou, A., & Hough, J., 2005, ASPC, 343, 79
[16] Packham, C., & Jones, T. J., 2008, SPIE, in press
[17] Packham, C., & Telesco, C. M., 2007, RMxAC, 29, 9
[18] C. Oh and M.J. Escuti, Physical Review A 76, 043815, 2007
[19] M J Escuti, C Oh, C Sanchez, C W M Bastiaansen, and D J Broer, Proc. SPIE 6302, 630207, 2006
[20] J. Tervo and J. Turunen, Optics Letters 25, 785-786, 2000
[21] S. M. Kelly, Journal of Material Chemistry 5, 2047-2061, 1995
[22] M. Schadt, H. Seiberle, and A. Schuster, Nature 381, 212-215, 1996
[23] M. J. Escuti and W. M. Jones, Proc. SPIE 6332, 633222, 2006
[24] J. Kim, C. Oh, M.J. Escuti, L. Hosting, ad S. Serati, Proc. SPIE 7063, in press 2008
[25] R.K. Komanduri, C. Oh, M.J. Escuti, and D.J. Kekas, SID Symposium Digest 39**,** 18-3, 2008
[26] Perrin, M. D., Graham, J. R., & Lloyd, J. P., 2008, PASP, 120, 555
[27] C. Oh and M.J. Escuti, Optics Letters, submitted, 2008
[28] C. Oh and M. J. Escuti, Optics Express 14, 11870-11884, 2006
[29] J. A. Fagan, J. R. Simpson, B. J. Landi, L. J. Richter, I. Mandelbaum, V. Bajpai, D. L. Ho, R. Raffaelle, A. R. Hight Walker, B. J. Bauer, and E. K. Hobbie, Physical Review Letters 98, 147402, 2007
[30] D.J. Broer, J. Boven, G. N. Mol, and G. Challa, Makromol. Chem., 1989, 190, 2255-2268
[31] Dowell, C. D., Davidson, J. A., Dotson, J. L., Hildebrand, R. H., Novak, G., Rennick, T. S., & Vaillancourt, J. E., 2003, SPIE, 4843, 250